Since January 2020 Elsevier has created a COVID-19 resource centre with free information in English and Mandarin on the novel coronavirus COVID-19. The COVID-19 resource centre is hosted on Elsevier Connect, the company's public news and information website.

Journal of Hazardous Materials 435 (2022) 129075

Contents lists available at ScienceDirect

Journal of Hazardous Materials

journal homepage: www.elsevier.com/locate/jhazmat

In-duct grating-like dielectric barrier discharge system for air disinfection

Liyang Zhang [a], Yuntao Guo [a,*], Xuanyu Chang [b], Zenghui Yao [c], Xiaodong Wei [b], Zihao Feng [a], Dongheyu Zhang [a], Qun Zhou [d], Xinxin Wang [a], Haiyun Luo [a,*]

[a] Department of Electrical Engineering, Tsinghua University, Beijing, China
[b] Marine Design and Research Institute of China (MARIC), Shanghai, China
[c] School of Electrical and Electronic Engineering, North China Electric Power University, Beijing, China
[d] Department of Chemistry, Tsinghua University, Beijing, China

HIGHLIGHTS

- In-duct grating-like DBD disinfectors suitable for HVAC systems were established and evaluated.
- The one-pass efficiency reached 99.8% with a pressure drop of < 20 Pa of the system, at the velocity of 0.5 m/s.
- Bactericidal efficiency was linearly correlated to the discharge power, regardless of the electrode arrangements.
- Gaseous short-lived chemical species or charged particles were major agents accounting for airborne bacteria inactivation.

GRAPHICAL ABSTRACT

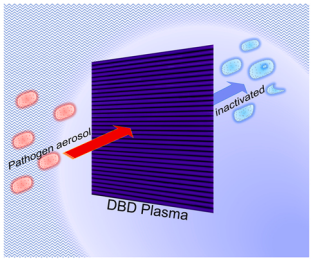

ARTICLE INFO

Editor: Dr. Danmeng Shuai

Keywords:
Dielectric barrier discharge
Air disinfection
In duct
HAVC system

ABSTRACT

In the context of spreading Coronavirus disease 2019 (COVID-19), the combination of heating, ventilation, and air-conditioning (HVAC) system with air disinfection device is an effective way to reduce transmissible infections. Atmospheric-pressure non-equilibrium plasma is an emerging technique for fast pathogen aerosol abatement. In this work, in-duct disinfectors based on grating-like dielectric barrier discharge (DBD) plasmas with varied electrode arrangements were established and evaluated. The highest airborne bacterial inactivation efficiency was achieved by 'vertical' structure, namely when aerosol was in direct contact with the discharge region, at a given discharge power. For all reactors, the efficiency was linearly correlated to the discharge power (R^2 =0.929–0.994). The effects of environmental factors were examined. Decreased airflow rates boosted the efficiency, which reached 99.8% at the velocity of 0.5 m/s with an aerosol residence time of ~3.6 ms. Increasing humidity (relative humidity (RH)=20–60%) contributed to inactivation efficacy, while high humidity (RH=70%−90%) led to a saturated efficiency, possibly due to the disruption of discharge uniformity. As suggested by the plasma effluent treatment and scavenger experiments, gaseous short-lived chemical species or charged particles were concluded as the major agents accounting for bacterial inactivation. This research provides new hints for air disinfection by DBD plasmas.

* Corresponding authors.
E-mail addresses: guoyt@tsinghua.edu.cn (Y. Guo), lhy@tsinghua.edu.cn (H. Luo).

https://doi.org/10.1016/j.jhazmat.2022.129075
Received 16 March 2022; Received in revised form 1 May 2022; Accepted 2 May 2022
Available online 6 May 2022

1. Introduction

Aerosol transmission is a non-negligible transmission route for a number of infectious agents such as respiratory viruses (influenza virus, respiratory syncytial virus, etc.) (Wang et al., 2021), airborne bacteria (nontuberculous mycobacteria, Legionella, etc.) (Fujiyoshi et al., 2017), and also the newly evolving severe acute respiratory syndrome coronavirus 2 (SARS-CoV-2) (Tang et al., 2020; World Health Organization, 2020), which gives rise to the Coronavirus disease 2019 (COVID-19) worldwide pandemic. SARS-CoV-2 aerosol is known to keep viable in the air with a half-life of 1 h (van Doremalen et al., 2020). The effective removal of pathogenic aerosol is thus crucial to minimize the potential dissemination risks.

Apart from wearing masks and physical distancing, appropriate ventilation is generally recommended by authorities. As evidenced by both occurred cases (Vernez et al., 2021; Jiang et al., 2020; Miller et al., 2021; Hwang et al., 2021) and simulation (Li et al., 2021), insufficient ventilation may lead to cluster outbreaks. Guidelines include the increase of air exchange rates by natural or mechanical ventilation in the enclosed spaces and less use of air recirculation (Blocken et al., 2021; World Health Organization, 2021). For heating, ventilation, and air-conditioning (HVAC) systems, complementary to ventilation, the insertion of air-cleaning devices in centrally connected units (Pease et al., 2021; Mihai and Rusu, 2021) or together with portable cleaners in distributed rooms (Blocken et al., 2021; Ren et al., 2021), is believed to be an efficient manner to reduce aerosol particles and also the potential cross infections. This work mainly focuses on in-duct disinfectors.

The most commonly applied duct air purification or disinfection techniques are fibrous filter (Azimi and Stephens, 2013; Xiang et al., 2021; Zaatari et al., 2014) and electrostatic precipitator (ESP) (Kim et al., 2013, 2019; Mo et al., 2020), while germicidal UV (Walker and Ko., 2007; Lee and Bahnfleth., 2012; Qiao et al., 2021; Luo et al., 2021) is also recommended. MERV 13 and high-efficiency particulate air (HEPA) filters have $>$ 85% and $>$ 99.97% single-pass filtration efficiency for the most penetrating 3-μm particles, respectively, but both have large air resistance and high energy consumptions (Zaatari et al., 2014; Faulkner et al., 2022). ESPs can achieve 50–95% removal efficiency for submicron particles (Kim et al., 2013) and improved ESPs can reach 90–99.5% (Kim et al., 2019; Mo et al., 2020). Filters and ESPs share disadvantages of timely maintenance (replacement or cleaning). Also, the potential risks of secondary infections cannot be ignored. For instance, bioaerosols may accumulate and even proliferate in the filter, making the filter a new source of contaminants (Möritz et al., 2001). Meanwhile, the disinfection efficiency of ESPs is rarely reported (Feng et al., 2021). For in-duct UVC disinfection, the irradiation output and the corresponding inactivation rate constant of conventional mercury-based UV lamps are seriously affected by air velocity, temperature, and humidity (Luo and Zhong, 2021). Meanwhile, the studies on light-emitting diode (LED)-based UV lamps are still on the way (Kim et al., 2018).

Non-thermal plasma (NTP) is a newly appearing technique for air disinfection (Gallagher et al., 2007; Wu et al., 2015; Lai et al., 2016; Xia et al., 2019; Nayak et al., 2020; Prehn et al., 2020). In the past decade, it has been proved to effectively inactivate bioaerosols including bacteria (*E. coli*, *P. fluorescens*, *B. subtilis*, etc) (Gallagher et al., 2007; Liang et al., 2012b)., viruses (MS2 phage, porcine reproductive and respiratory syndrome virus [PRRSv], Newcastle disease virus [NDV], etc) (Wu et al., 2015; Xia et al., 2019; Schiappacasse et al., 2020), as well as SARS-CoV-2 RNA aerosol (Bisag et al., 2020), with major advantages of low residence time (~ms) and low pressure drop (<20 Pa) (Lai et al., 2016; Xia et al., 2019). Regarding air plasmas, a cock tail of reactive oxygen and nitrogen species (RONS) are initiated by accelerated electrons and generated in short times (10^{-7}-10^{-3} s) through complex gaseous reactions (Sakiyama et al., 2012; Tian and Kushner, 2014). For surface and liquid decontamination, RONS plays a major role in bactericidal effects in most cases (Guo et al., 2015). In terms of air disinfection by NTP, however, there is limited knowledge on (i) germicidal factors; (ii) the influence of ventilation duct conditions; (iii) the correlation between plasma discharge and disinfection efficiency, let alone dose behaviors or inactivation kinetics. To sum up, the long-lived ozone was reported not to be the major inactivating factor (Vaze et al., 2010) and short-lived species were suspected as the dominant or necessary contributors (Nayak et al., 2020; Prehn et al., 2020; Vaze et al., 2010). In the case of a high ozone concentration (80 ppm), the indirect (exposed to long-lived species) and direct plasma treatment could yield similar inactivation effects (Schiappacasse et al., 2020). Bacterial cell membrane disruption after plasma treatment was generally observed (Liang et al., 2012a, 2012b; Park and Hwang, 2013; Romero-Mangado et al., 2017, 2016). Higher humidity usually impairs disinfection effects (Lai et al., 2016; Xia et al., 2020), whereas the influence of airflow rates on inactivation efficiency is controversial. Higher flow rates may promote bacterial or reduce viral inactivation (Lai et al., 2016; Xia et al., 2020). Accordingly, the influence of environmental factors should be clarified. Additionally, most previous studies are on a laboratory scale, with small device sizes and thus relatively low airflow rates of 0.6–4 (Bisag et al., 2020; Park and Hwang, 2013), 10–28 L/min(Wu et al., 2015; Liang et al., 2012b; Schiappacasse et al., 2020), and 125–340 L/min(Xia et al., 2019; Prehn et al., 2020; Xia et al., 2020), which is not or less supportive of its use in practical HVAC systems, which generally require flow rates of at least 500–1000 L/min (or higher).

In this work, we established and evaluated different structures of grating-like DBD reactors. Both the discharge characteristics and bactericidal effects were considered. The one-pass antibacterial efficiency regarding input power, airflow velocity, humidity, power source, and bacterial species were examined and the potential germicidal factors including aqueous species in bacterial droplets, gaseous long-lived species, UV radiation were investigated.

2. Materials and methods

2.1. DBD reactor setup

Fig. 1A shows the schematic of the DBD reactors used in this work. Inspired by a previous report (Gallagher et al., 2007), the basic unit of the reactors is a 2-mm diameter copper rod shielded with a quartz tube with inner and outer diameter of 2 mm and 4 mm, respectively. Presuming that the relative positions of discharge and aerosol motion track could influence the aerosol inactivation, a total of six reactors were designed. The electrodes were installed in a dielectric holder made of phenol-formaldehyde (PF) resin. All air gaps between high-voltage and grounded electrodes were kept at 1 mm. As shown in Fig. 1A, 'parallel' and 'vertical' depict the direction of airflow, which is parallel or perpendicular to the discharge filament, respectively. For the 'hybrid' structure, in theory, the direction of discharge filament is stochastic, both parallel and perpendicular are possible. Concerning 'vertical-1' structure, the second layer is only assembled by quartz tubes with no electrodes in. Regarding 'staggered' structures, the electrodes in the backward layer are vertically staggered from the front one. Such configuration alters the flow field and may contribute to disinfection. The pressure drop across the reactor was measured by a digital manometer (DP-CALC 5825, TSI). It isfound that the six reactors have a close pressure drop (Fig. S1). As from the curve fitting, the functional relation between pressure drop (denoted as Pd) in Pa and inlet airflow velocity (denoted as v) in m/s can be simply illustrated as $Pd = 17.72 \times v^2$ ($R^2 = 0.9995$). At 1 m/s of velocity, the pressure drop is about 18 Pa, which is about 1/4–1/3 of a HEPA filter with similar sizes.

The plasma reactor was driven by a sinusoidal-alternating-current (AC) generator (CTP-2000 K, Nanjing Suman) or a pulsed power source at a frequency of 1 kHz. The pulsed power source was only used in section 3.2.3. Under the AC-driven, the discharge appearance was imaged by a Cannon camera with a 30 s exposure time. As for the vertical-1 structure, discharge is ignited in most regions except locations with larger gaps at 8 kVp of applied voltage (Fig. 1A). Such unevenly

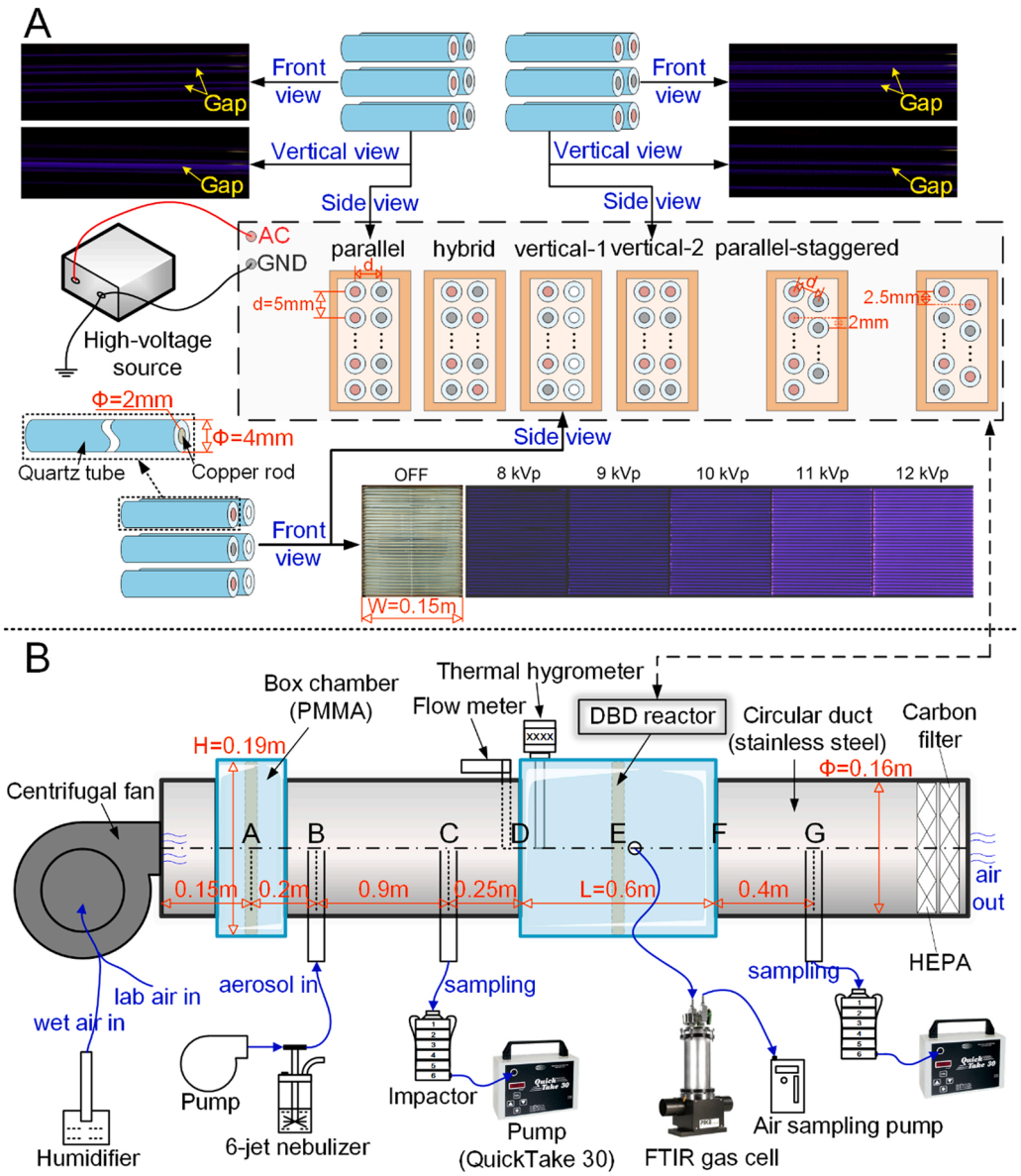

Fig. 1. Schematic diagram of (A) DBD reactors and (B) the ventilation duct system for one-pass efficiency test. In the front view of the 'parallel' reactor and the vertical view of the 'vertical-2' reactor, weak light emission can be observed at the edges of the quartz tubes due to the light reflection and/or refraction.

spaced gaps could hardly be avoided due to the limited accuracy of manufacturing. At higher voltages, the discharge is much more uniform. For vertical-2 and parallel structures, we used three pairs of electrodes to illustrate the discharge position. The applied voltage is 9 kVp at a frequency of 1 kHz. As is shown in Fig. 1A, discharge happens between the adjacent high-voltage and grounded electrodes, while no diagonal discharge is observed.

2.2. Plasma characterization

The characteristics of the plasma discharge filaments and the optical emission were examined. A pairwise-electrode DBD unit held by two transparent quartz plates with an air gap of 1 mm was built to better visualize the filaments (Fig. 2A). The discharge inception voltage is about 7.1–7.2 kV. The images of the discharge in side and front views were captured by an ICCD camera (PIMAX2, Princeton Instruments). For illustration, the vertical-1 reactor was used to acquire plasma emission characteristics. The optical emission spectra were obtained by using an optical fiber connected to a two-channel spectrometer (MX2500+, Ocean Optics) (Zhang et al., 2021) with 0.1 nm resolution. A total of 10 gaps were measured at a spatial step of 0.5 mm with a randomly selected starting point. The exposure time is fixed at 30 s to obtain signals with moderate intensities.

2.3. Experimental setup

The bacterial aerosol removal efficiency with one pass through the discharge reactor was measured by a homemade ventilation duct test system. The schematic of the experimental test system is shown in Fig. 1B. The duct is spliced by three circular stainless-steel tunnels with an inner diameter of 160 mm and two rectangular chambers made of polymethyl methacrylate (PMMA) with an inner height of 190 mm and width of 180 mm. The transparent chamber enables the visualization of the discharge. The DBD reactor can be placed either at location A or E (Fig. 1B). The duct airflow velocity was regulated by a frequency-control centrifugal fan and monitored by a hot-wire anemometer (405i, Testo) with the detector placed at the center of the duct (~5 cm before location D). The experimental airflow velocity was controlled at 0.5, 1, 2, and

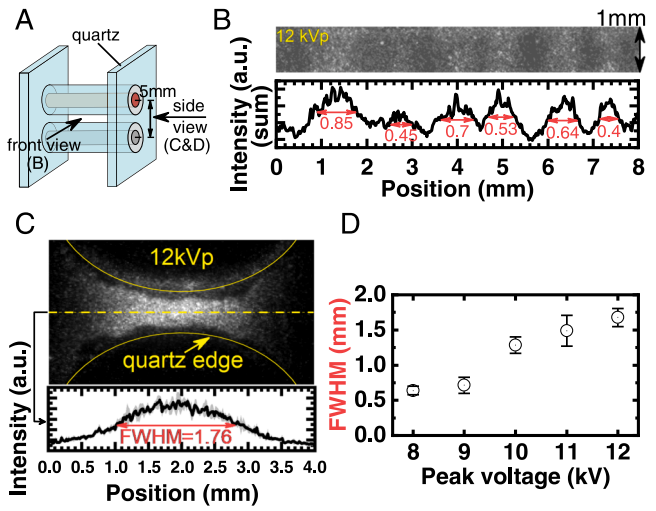

Fig. 2. ICCD images of discharge filaments. (A) Schematic diagram of the pairwise-electrode DBD unit. (B) and (C) Discharge filaments in the front and side views with 1-ms exposure time. The full width at half maxima (FWHM) parameter of filaments from the side view as a function of applied voltages is given in (D).

3 m/s, which almost covers the common HVAC operating conditions. The corresponding Reynolds number of the inlet flow in the circular duct is estimated to be 5700–34400, indicating a turbulent flow. The radial velocity at the positions 1 cm away from the duct surface was measured close to the value in the center (difference<8%). Therefore, the flow rate can be simply estimated by multiplying the central velocity and the cross-section area. The flow rate is about 145 m^3/h (or 2400 L/min) at a central velocity of 2 m/s. The temperature and relative humidity (RH) of the inlet flow were measured by a thermal hygrometer (605-H1, Testo) and the temperature was maintained between 18 and 22 ℃ by the air-conditioning units in the lab, while the RH was adjusted by a humidifier. The temperature of the plasma reactor during discharge was monitored by an infrared thermal camera (E4, FLIR). Due to the fast air cooling, no significant temperature rising (<10 ℃) was observed throughout the experiments. A commercially available activated carbon filter and a HEPA filter were placed at the end of the duct to eliminate the ozone and bacteria emissions, respectively.

The bacterial suspension was aerosolized by a 6-jet nebulizer (Collision, BGI) and fed into the center of the duct at location B with inlet airflow of 13–16 L/min. The upstream (location C, ~0.55 m to the reactor) and downstream (location G, ~0.7 m to the reactor) airborne bacteria were separately and simultaneously sampled by two six-stage Anderson cascade impactors (Beijing Mingjielantian Technology Co., Ltd) with a flow rate of 28.3 standard liter per minute (SLM) and sampling time of 1 min.

The waveforms of voltage and current were measured by a high voltage probe (6015 A, Tektronix) and a current monitor (TCP312A, Tektronix), respectively. Under the condition of the AC source, a 100-nF capacitor was in series connection with the reactor to calculate the discharge power by the Lissajous method (Guo et al., 2021), whereas for the pulsed power source, the power was calculated by integrating the product of voltage and current. The long-lived species in the plasma treated gas (effluent) was measured by a 4.2-m gas cell equipped in a Fourier Transform infrared (FT-IR) spectrometer (Frontier, PerkinElmer) with a deuterated tri-glycine sulfate (DTGS) detector. The spectra were recorded with 16 scans to reduce noises. To avoid the potential water intervention, the effluent was first introduced to a $CaCl_2$-filled drying pipe and then into the gas cell at a flow rate of 1 L/min. The length of the air sampling tube from the sampling port (~5 cm behind the reactor) to the gas cell is about 0.5 m. The concertation of O_3 in the effluent was also quantified by the UV absorption method using a mercury lamp as the UV light source (Guo et al., 2021). The detector was placed ~5 cm behind the reactor with an optical path of 10 cm. Thus, the ozone concentration measured by the UV method is a spatial average.

2.4. Experimental procedure

Gram-negative *E. coli* (ATCC 8099) and gram-positive *S. albus* (ATCC 8032) were selected as the tested bacteria. The bacteria strains were streaked and incubated on nutrient agar slants overnight for 13 h and then harvested and washed with 0.9% (w/v) saline. The initial bacterial concentration is 5–10 × 10^9 colony-forming units (CFU) per milliliter. Next, the suspension was diluted to 10^5–10^6 CFU/mL, 30 mL of which was used for nebulization. The solution nebulization rate was 0.2–0.4 mL/min. The bacteria in the duct was maintained in the range of 5000–25000 CFU/m^3. The airborne bacteria were collected on the agar plates placed in the stages of the impactor. Then the plates were incubated at 37 °C for 24 h and then counted. The single-pass bacterial removal efficiency is calculated according to the China's standard *Air Cleaner for Ventilation System* (GB/T 34012-2017) (The Standardization Administration of the People's Republic of China, 2017):

$$E_w = \frac{N_u - N_d/(1-\eta)}{N_u}, \text{ where } \eta = \frac{N_u^{'} - N_d^{'}}{N_u^{'}}$$

Where $N_u^{'}$ and $N_d^{'}$ represent the total CFU (by summing up all stages) of upstream and downstream bacteria with an empty duct, while N_u and N_d denote the CFU with the reactor in the duct, respectively. The parameter η denotes the natural survival decaying of aerosols without the influence of plasma reactor, which may arise from aerosol drying or the potential systematic error due to the flow field distribution. Such an influence could be corrected by dividing N_d by $1-\eta$. Unless stated otherwise, we used *S. albus* to test the performance of plasma reactors. For each condition, the experiments were repeated at least four times.

3. Results

3.1. Plasma characterization

3.1.1. Discharge filaments

The formation of multiple discharge filaments is the typical phenomenon of atmospheric pressure air DBD plasma (Chirokov et al., 2004). The size and the distribution of filaments are the fundamental knowledge of DBD and the generation of reactive species. To better visualize the filaments, the pairwise-electrode DBD unit was used and the voltage was fixed at 12 kVp. As shown in Fig. 2B, even with 1-ms exposure, the filaments are not uniformly distributed in the gap. This can be explained by the 'memory effect' of DBD, that is, discharge is prone to form at the same spot of the last microcharge once the voltage polarity is inverted, due to the remaining deposited charges (Fridman et al., 2005). Note that the duration of a single microcharge is about 1–20 ns. Therefore, these filaments are the accumulation of multiple microcharges, tens of, for example. Generally, the radius of the accumulative filaments is about 0.4–0.8 mm from the front view (Figs. 2B) and 1.5–1.7 mm from the side view (Fig. 2C and D). More images can be found in Fig. S2.

3.1.2. Optical emission spectra

It is found that the emission spectra vary almost periodically in line strength across gaps (data not shown). The variation of the strongest line at around 337 nm, which corresponds to 0–0 vibrational transition of N_2(C-B) (Staack et al., 2005b) is given in Fig. 3A. The intensity fluctuates around 1600 (a.u.) across the ten gaps, suggesting a repeatable and periodic discharge across gaps in terms of a 30-s exposure time. For a single spectrum as shown in Fig. 3B, the emission bands are dominated by the second positive system of molecular nitrogen (Staack et al.,

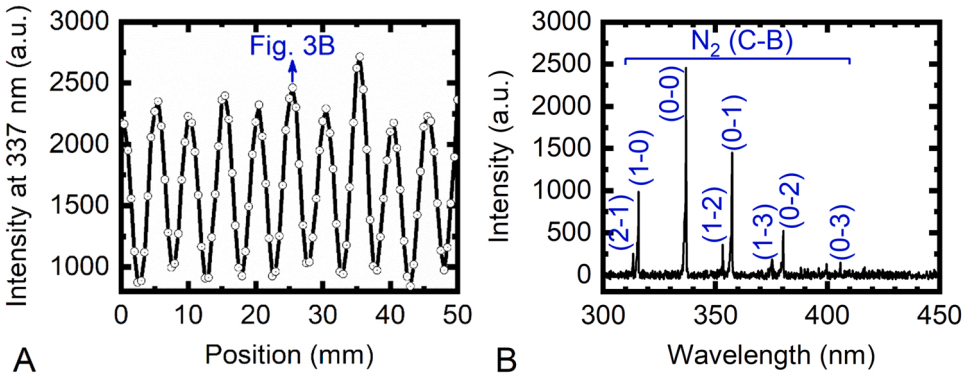

Fig. 3. Optical emission characteristics of the vertical-1 reactor under 12-kVp AC voltage and ~20% RH. (A) Emission intensity at around 337 nm at a line across 10 gaps, (B) Typical spectrum in the range of 300–450 nm.

2005a), while no ·OH lines (306–312 nm) or oxygen atom (777 or 844 nm) is observed.

3.1.3. *Electrical parameters*

The power consumption of the six reactors as a function of applied voltage was first measured. As illustrated in Fig. 4A, for all reactors, the discharge power is roughly exponentially increased with rising applied voltage. Except vertical-1 reactor whose power is almost half of the vertical-2, other ones share close discharge power. Note that the vertical-1 reactor has only one less gap than the parallel but the corresponding discharge power is much lower. The possible cause is the accumulation of electrical charges on the dielectric, which may weaken the electrical field and also the discharge of the adjacent air gap.

Hereinafter, the vertical-2 structure with a constant applied voltage of 10 kVp was taken as an example to examine the influence of humidity. As shown on the left axis of Fig. 4B, the power initially decreases slowly with RH values in 20–60%, reaching a local minimum of 25.5 W, and then rises up at higher RH values. The discharge current waveforms as a function of humidity are shown in Fig. S3. The root mean square (RMS) current (I_{RMS}) was calculated (method see (Nguyen et al., 2020)) and presented on the right axis of Fig. 4B. It is found that the variations of I_{RMS} are similar to that of discharge power. Note that the parameter I_{RMS} considers not only the conduction current but also the displacement current. Thus, the variation of I_{RMS} is less pronounced than the discharge power. The decreasing of current and discharge power in 20–60% RH can be attributed to the electro-negative property of water gas (Takaki et al., 2021), while at higher RH levels, water may deposit on the dielectric surface, increasing the surface conductivity and thus current and power consumption (Nguyen et al., 2020; Deng et al., 2020).

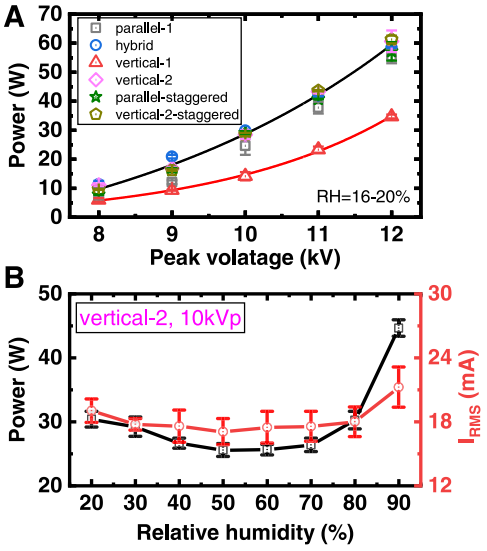

Fig. 4. (A) The power consumption of the six reactors as a function of peak voltage at RH values of 16–20%. (B) The power and RMS current of vertical-2 reactor as a function of RH values. The power and current were measured three times, each time including three replicates of periods.

3.2. *Airborne bacteria inactivation: influential factors*

3.2.1. *Electrode configuration*

To enable comparison among the plasma reactors, the airflow velocity is fixed at 2 m/s and RH at 16–20%. Note the velocity here describes the inlet airflow, not the airflow in air gaps inside the discharge reactor, which should be larger. The residence time of bacterial aerosol in the discharge reactor is roughly estimated by dividing the five times (air-facing total area dived by air gap area) of inlet airflow velocity into the depth of the reactor. For 'vertical-2′ reactor, the residence time is about 0.9 ms at 2 m/s of inlet airflow.

The one-pass efficiency of viable bacteria of different reactors as a function of the applied voltage is given in Fig. 5. As is presented, when plasma is off, the efficiency is between 3% and 6%. This may arise from physical filtration and/or flow field disturbance after the reactor is installed. Therefore, the tested one-pass efficiency is dominated by inactivation rather than physical removal. Overall, the vertical-2 reactor achieves the best bactericidal effect, vertical-1 encountered the worst, whereas parallel structure has close reduction rates to the hybrid structure. The strong dependence of removal efficiency on input power is shown in Fig. 5B. The averaged scattering data were best fitted by linear curves with R^2 values of 0.929–0.994. Compared to other reactors, vertical-1 reactor only has one discharge layer, namely a half interacting residence time with plasma discharge, and thus it is not included in Fig. 5B. The effects of reactors with three or more layers are not tested because of the limited power source output. In the following context, to simplify, the vertical-2 DBD reactor was used to probe the effects of environmental factors, power sources, and the corresponding germicidal factors.

3.2.2. *Airflow velocity and humidity*

As presented in Fig. 6A, the bactericidal efficiency decreases with increasing velocity, best at 0.5 m/s with an efficiency of 73.5–99.8% at 8–12 kVp. Note that such a low airflow velocity has negligible influence on the air discharge due to the fast electron avalanche (~ns) processes. A higher airflow rate leads to a shorter residence time of aerosols in the discharge region and thus a low inactivation efficiency. At inlet airflow of 0.5 m/s, the residence time is roughly estimated to be 3.6 ms. As for the influence of humidity, the inactivation efficiency increased from 37% to 87% when the RH level increases from 20% to 70% and reaches saturation at higher RH levels (70–90%). Such a saturation phenomenon

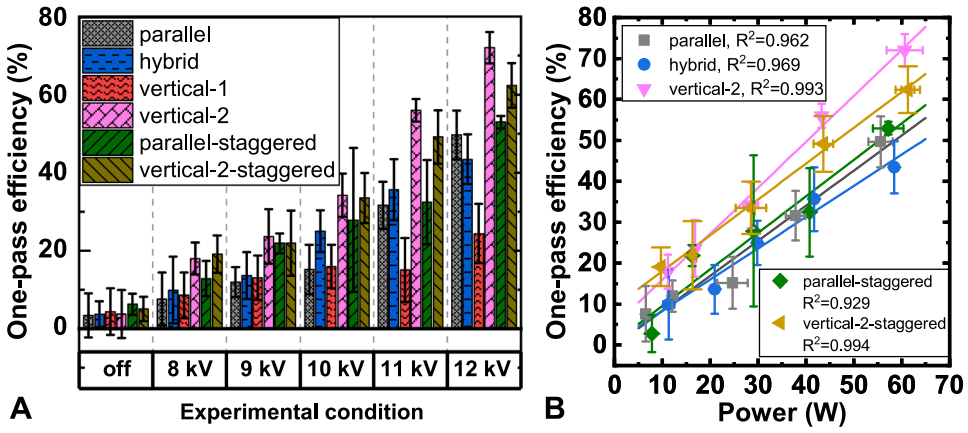

Fig. 5. One-pass efficiency of the plasma reactors as a function of (A) applied peak voltage and (B) discharge power. Conditions are: airflow velocity of 2 m/s and RH value of 16–20%.

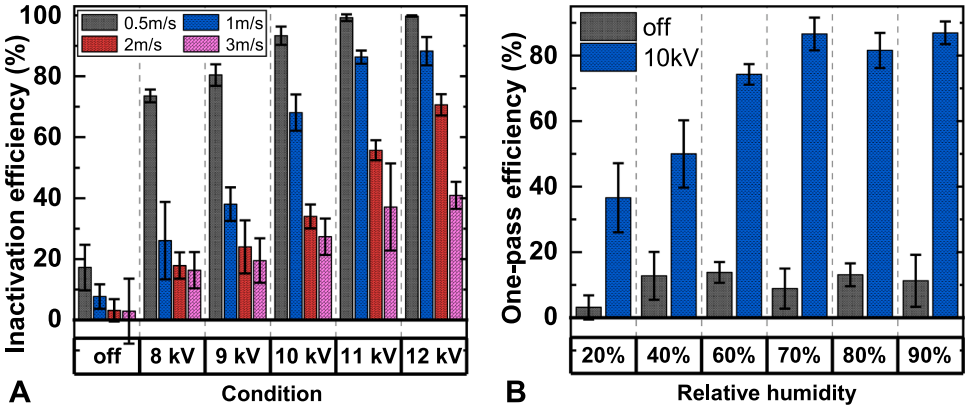

Fig. 6. The impact of (A) airflow velocity and (B) RH values on the one-pass inactivation efficiency of vertical-2 reactor. Conditions: RH of 16–20% (A), voltage of 10 kVp and airflow velocity of 2 m/s (B).

can be partially explained by the disruption of discharge uniformity under high humidity (>60%), as indicated by the discharge photos (Fig. S4).

The contributing role of humidity on surface decontamination by air plasmas has been widely reported (Hähnel et al., 2010; Ki et al., 2019; Patil et al., 2014; Kogelheide et al., 2020a), and the causes are usually attributed to the higher concentration of ·OH and peroxides (H_2O_2, etc.) at high RH levels, which has been predicted by numerical models (regarding corona discharge) (Junhong and Pengxiang, 2005; Nakagawa et al., 2011; Komuro et al., 2013a) and observed by experiments (Ki et al., 2019; Patil et al., 2014). However, for airborne bacteria inactivation, the role of humidity is rarely reported. As from a report by Lai et al. who also employed a DBD device, a much lower inactivation efficiency of *E. coli* and *S. epidermidis* was observed at a high humidity level (RH=81%) compared to a low level (RH=50–60%) (Lai et al., 2016). We speculate that this could be the result of a lower voltage output at higher RH levels due to the increased device capacitance, assuming an unchanged input. In other words, the electrical matching between the discharge device and power source under high RH levels should be taken into consideration. In another report, the authors used packed bed plasma to inactivate porcine reproductive and respiratory syndrome virus (PRRSv) and they found the efficiency was decreased by almost a half under RH value of 49% in August compared to 38% in May (Xia et al., 2020). They assumed the cause as the accumulation of virus stock in the packed bed under higher RH levels. Inferring from such a result, packed bed plasma may suffer from the disadvantage of being sensitive to environmental humidity. From this perspective, the grating DBD device in this work is better tolerated in a humid environment.

3.2.3. Power sources and bacterial species

Pulsed power source is widely used in recent years for its low thermal effects and high production rates of reactive species, suitable for biomedical applications (Zhang et al., 2013, 2020b). Here, the bactericidal effect of nanosecond pulse plasmas was examined. The voltage and current waveforms are given in Fig. S5. The frequency is 1 kHz, same as the AC supply, while the peak voltages at 'input-1′ and 'input-2′ are 9.4 and 11.6 kV, respectively. The bacterial survival curve is shown in Fig. 7A. The reduction rates are 10–15% for the two inputs with the discharge power of 0.8–1.8 W. Note that compared to 'input-1′, the efficiency even has a little reduction at 'input-2′. This is likely due to the experimental errors caused by the low duty cycle of the pulsed source. The duration of the high-voltage output is several μs (Fig. S5), far less than the time period of 1 ms and also the residence time of bacterial aerosols. In other words, the meeting of bacterial aerosol with germicidal factors is highly stochastic. Nevertheless, pulsed-driven DBD yields a much better efficiency than AC-driven one at the same power level. However, pulsed power source usually has the shortcomings of low load capacity (~pF) and high costs. Therefore, it may be not applicable for practical use, in view of the large capacitance of in-duct DBD devices (e.g., hundreds of pF).

Next, the removal efficiency of *E. coli* and *S. albus* were examined and compared at the same applied AC voltage of 12.5 kVp and 930 Hz. As shown in Fig. 7B, the reduction of the two species of bacteria is rather close, both reaching 90%. Note that the susceptibility of different bacteria to the plasma treatment is not always close, according to the previous reports. For instance, *E. coli* K12 is more susceptive than *E. coli* 21181 (Prehn et al., 2020), while *M. luteus* is much more resistant than

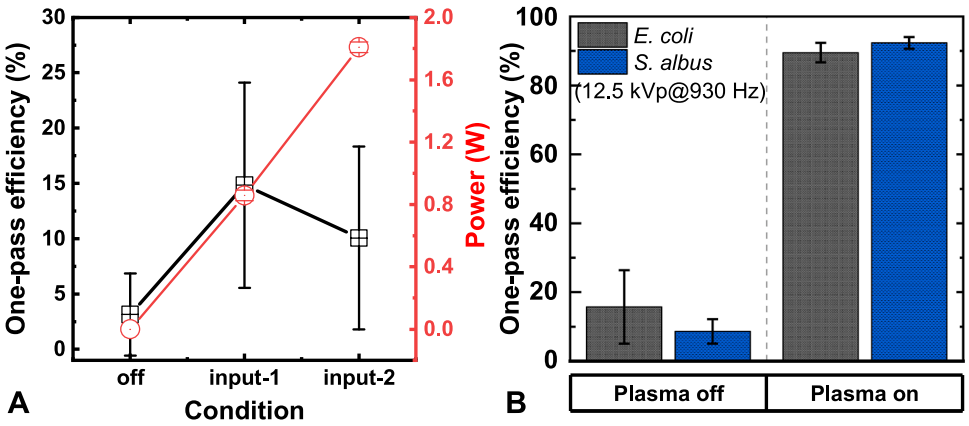

Fig. 7. One-pass efficiency of (A) *S. albus* treated by nanosecond pulse DBD and (B) *E. coli* and *S. albus* treated by AC source at 12.5 kVp and 930 Hz. The power of the pulsed source is shown on the right axis (A). 'Input-1' and 'input-2' correspond to peak voltages of 9.4 and 11.6 kV, respectively (A). Conditions are: vertical-2 reactor, airflow velocity of 2 m/s, and RH values of 16–20% (A and B).

E. coli and *S. epidermidis* (Lai et al., 2016). Such difference may be due to the varied capabilities of bacteria to respond to the oxidative stress induced by reactive species.

3.3. Airborne bacteria inactivation: potential mechanisms

3.3.1. Role of aqueous species

Considering the potential liquid environment surrounding bacteria in the aerosolized droplets, aqueous species were first considered to interpret the bactericidal mechanisms. Due to the small size and high specific surface area of droplets, short-lived species like ·OH and $^1O_2$ may play an important role (Gao et al., 2021), whereas long-lived species may also play a role. In this work, we intend to vary the aqueous environment in droplets by adding reagents to the bacterial stock prior to aerosolization. Phosphate buffer solution (PBS) was used to maintain the pH value, scavengers including L-histidine, D-mannitol, sodium pyruvate, ascorbic acid, or glutathione (GSH) were applied to quench specific species (Aboubakr et al., 2016), while bovine serum albumin (BSA) was utilized as interference, respectively. Scavengers were adjusted to a final concentration of 10 mM and BSA to 5 mg/mL. Note that the 10-mM concentration is high enough to deactivate the target species (mainly ROS), whose concentration is usually on the order of μM-1 mM with minutes of treatment (Wu et al., 2012; Ghimire et al., 2018; Lukes et al., 2014). Besides, higher concentration could lead to unexpected bacterial death.

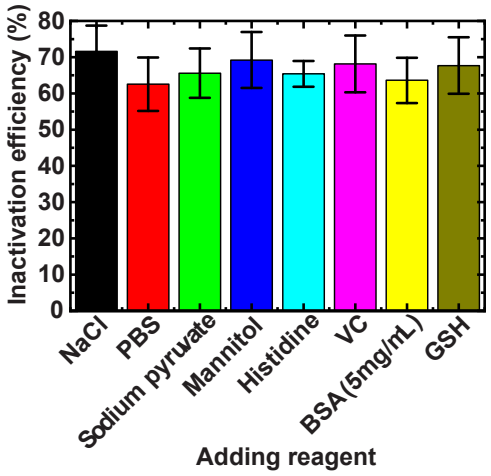

Fig. 8. The influence of adding reagents on aerosol inactivation. Conditions are: vertical-2 DBD reactor, applied voltage of 12 kVp, inlet airflow velocity of 2 m/s, and RH of 16–20%.

The results are shown in Fig. 8. Clearly, compared to NaCl (i.e., no reagent added), all adding reagents lead to a slight but not significant drop in survival reduction rates. Such results require a reevaluation of the role of aqueous species. We know that water content in the droplet is determined by the evaporation and agglomeration processes and we assume that duct airflow may contribute to the evaporation of the droplet, resulting in a relatively dry environment around the bacteria. In turn, we infer that gaseous species are the major germicidal factors rather than aqueous species.

3.3.2. Role of gaseous long-lived species

The role of gaseous long-lived species was evaluated hereinafter. The discharge effluent was first analyzed by the FT-IR gas cell to inspect the long-lived species. As seen from the infrared spectra in Fig. 9A, the long-lived species are dominated by O_3 (bands at 1055 and 2120 cm^{-1}) (Pavlovich et al., 2014) and NO_2 (band at 1630 cm^{-1}) (Pavlovich et al., 2014), while both species rise with increasing voltage (Fig. 9B). The O_3 concentration is 5–6 ppm at 12 kVp as measured by the UV absorption method, which is close to or lower than the reported values of 5–80 ppm (Gallagher et al., 2007; Prehn et al., 2020; Schiappacasse et al., 2020; Park and Hwang, 2013).

Next, the reactor was placed at location A (in front of the aerosol inlet, Fig. 1B) and the efficiency was also calculated based on upstream and downstream sampling to denote the effects of effluent. Note such an efficiency corresponds to an effective length of 1.25 m (location C to G, ~625-ms duration), which is larger than 0.7 m (location E to G) when the reactor is installed at location E. Thus, the role of plasma effluent is overestimated. The efficiency as a function of voltage is given in Fig. 9C. The survival reduction rises from 5% to 20% at voltages of 8–12 kVp. Compared to direct treatment (vertical-2, Fig. 5 A), under which the reduction rates rise from 24% to 72%, one can conclude that long-lived species account for at most ~1/3 of total inactivation. The bactericidal effect of long-lived species generated by plasmas on aerosolized bacteria is rarely reported. Vaze et al. showed that the 10-s exposure to 28-ppm ozone resulted in 10% inactivation of airborne *E. coli* while direct exposure led to 97% of inactivation (Vaze et al., 2010). Note that both the exposure time and ozone concentration are much higher than those in this work. In turn, we assume that NO_x may play an important role. A report shows that the co-existence of O_3 and NO_2 in the plasma afterglow yields a much better viral inactivation efficiency than O_3 or NO_2 alone, possibly due to the formation of N_2O_5 (Moldgy et al., 2020).

The influence of RH levels on plasma effluent species was also examined. When the RH value is high as 40% or 60%, the long-lived species are also dominated by O_3 and NO_2 (Fig. 10A). The water absorption bands are obvious at 60% or higher RH values. Most likely,

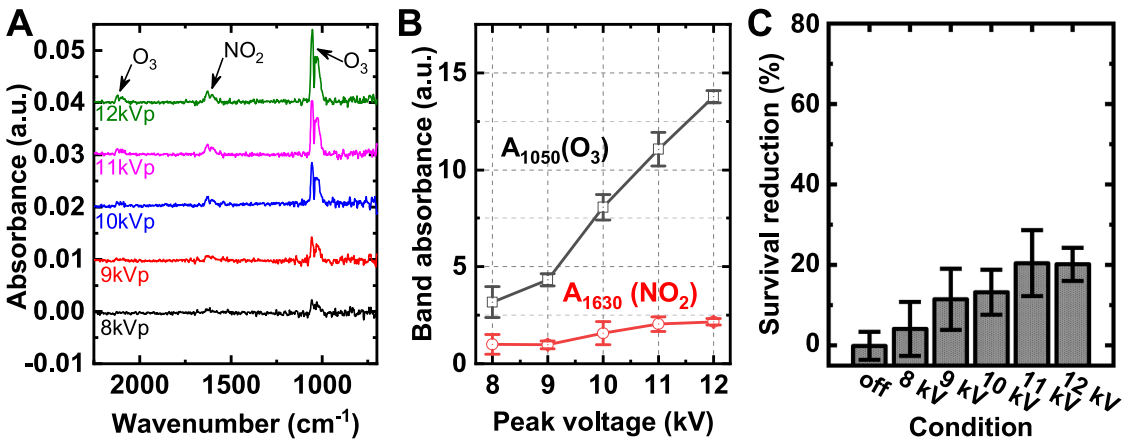

Fig. 9. The infrared spectra (A), band absorbance (B), and inactivation efficiency (C) of the plasma effluent as a function of applied voltage. Conditions are: vertical-2 reactor, airflow velocity of 2 m/s, and RH values of 16–20%.

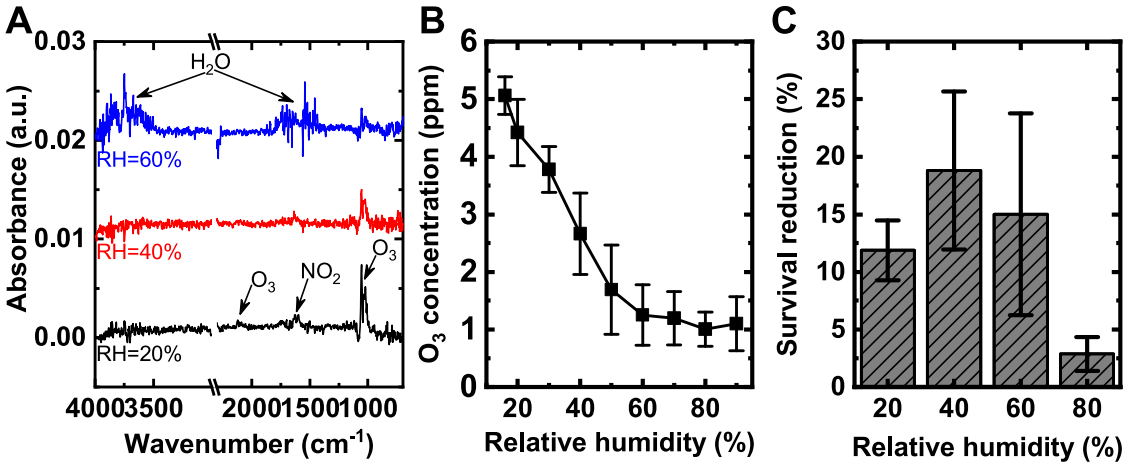

Fig. 10. The infrared spectra (A), O_3 concentration (B), and bacterial survival reduction rates (C) of the plasma effluent as a function of RH levels. Conditions are: vertical-2 reactor, airflow velocity of 2 m/s, and 10 kVp of applied voltage.

other long-lived species such as H_2O_2 or HNO_3, etc. are beyond the detection limit (~0.1 ppm) of the used 4.2-m FT-IR gas cell. Meanwhile, as measured by the UV absorption method, the ozone concentration decreases from 5.1 ppm to 1 ppm as RH increases from 16% to 60%. The ozone roughly reduces to a half at 45% of RH, compared to 20% of RH. The decreasing of ozone against humidity is usually attributed to the consumption of O and O_3 by radicals like·HO_2 and·OH in the discharge region (Junhong and Pengxiang, 2005; Zhang et al., 2016). When using plasma effluent for inactivation, the survival reduction first increases with RH and then settles down (Fig. 10C), which is not correlated to the ozone variations. Though not validated, H_2O_2 should play an important role. The concentration of H_2O_2 in the plasma effluent is known to increase at high RH values (Winter et al., 2014; Doležalová et al., 2016), which could lead to the higher efficiency at 40% of RH compared to 20%. However, at 60% and 80% of RH values, the discharge uniformity is disrupted, resulting in a possible reduction of H_2O_2 and thus low efficiency. Overall, the inactivation efficiency is lower than 20%. In comparison with those in Fig. 6B, the plasma effluent accounts for 5%–35% of the total inactivation.

4. Discussion

In view of air disinfection evaluation, the commonly applied sampling methods to collect airborne bacteria or viruses are cascade impactor (Lai et al., 2016; Park and Hwang, 2013) and liquid impinge (Nayak et al., 2020; Vaze et al., 2010). A possible concern should be taken into consideration when using liquid impinger for disinfection evaluation of plasma-based techniques because the plasma effluent is known to diffuse into or react with liquid, forming aqueous bactericidal species (e.g·H_2O_2, O_3, nitrite/nitrate, ONOOH, etc) (Liu et al., 2015; Xi et al., 2020), which may lead to unexpected survival losses. As a report by Nayak et al. who used plate DBD for airborne viral inactivation, the concentration of NO_2^- and NO_3^- reached 10–80 μM and 0.1–1.7 mM in the sampled liquid, respectively (Nayak et al., 2020). Schiappacasse et al. reported the unexpected inactivation of NDV in the collected liquid media even after adding a high concentration of sodium sulfite, a scavenger of reactive oxygen species (Schiappacasse et al., 2020). In this respect, the Anderson impactor should be better because it collects bacteria directly on the agar plate surface. Another important issue comes with sampling efficiency. The impactor used in this work has a 50% cutoff diameter of 1.1 and 0.65 μm at the fifth and sixth stage, respectively. Results showed that most (>97%) bacteria were collected by the fifth and sixth stages, compared to the first to the fourth stage. That is, a three- or two-stage impactor with a proper cutoff diameter may also be applicable. A single sixth stage of Anderson impactor is reported with an approximate 90% sampling efficiency for *S. epidermidis* aerosol, which has a geometric mean diameter of 1.08 μm (Park and Hwang, 2013).

In the context of airborne pathogen inactivation by non-thermal plasmas, the germicidal factors may include UV radiation, charges

(electrons, ions), and gaseous/aqueous short or long-lived chemical species. The UV-C irradiance of the vertical-2 reactor at 12 kVp of applied voltage was measured by a UV light meter. The distance between the air gap and the UV detector is about 1 cm. The measured irradiance is less than 1 μW/cm^2, namely, the UV-C dose is on the order of nJ/cm^2 which is far less than the conventional UV-C dose (~mJ/cm^2) required for airborne bacterial inactivation (Qiao et al., 2021; Chang et al., 2013; Zhang et al., 2020a). Accordingly, the role of UV radiation could be excluded. Meanwhile, the role of charged particles cannot be ignored. The electron avalanche or streamer usually propagates at a velocity of 10^5-10^6 m/s (Komuro et al., 2013b). The drifting speed of ions in the discharge field in air is on the order of 10^3 m/s, assuming ion mobility of ~10^{-4} m^2/(V·s) (Nelson et al., 2003) and electrical strength of 10^7 V/m, while the aerosol particles swarm at the velocity of 1–10 m/s. Thus, charged particles may rapidly accumulate on the bacterial surface and finally lead to bacterial death through Coulomb repulsion or other effects. Additionally, as is illustrated in sections 3.3.1 and 3.3.2, aqueous species and long-lived chemical species may play a minor role in airborne bacterial inactivation. Therefore, one can conclude that short-lived chemical species or charged particles may play a major role. By comparing Fig. 4B with Fig. 6B, it seems that the relationship between the inactivation efficiency and current (or power) is not clear. That is, chemical species are more likely to be responsible for inactivation than charges under the condition of a high RH level.

For grating-like DBD, it is obvious that the electrode arrangement has non-negligible effects on the bacterial inactivation efficiency (Fig. 5). The vertical-2 reactors (staggered or not staggered) yield higher efficiency than other reactors, given an identical discharge power. Electrode arrangement determines the propagation direction of discharge and also how pathogen aerosol interacts with electrons, ions, and chemical species. As from the numerical models regarding surface DBD, the effective diffusion distance (EDL) of both ionic and short-lived species generated by discharge is less than 0.1 mm, corresponding to a lifetime of <100 μs (Sakiyama et al., 2012; Liu et al., 2015). Namely, the transport distance of short-lived species is limited, even if considering the local gas flow (~ m/s). Hence, for parallel or hybrid structure, the short-lived species are likely to be in less contact with bacterial aerosol, resulting in a lower disinfection efficiency. Further, to increase the discharge uniformity is another possible way to promote bactericidal efficiency. It is commonly acknowledged difficult to generate a homogenous discharge in atmospheric air (Ran et al., 2018). However, it is possible in theory to reduce the non-homogeneity of discharge simply by decreasing the gap or improving the electrical field distribution by varying the material or size of the dielectric.

NTP has been reported to effectively inactivate viruses on surfaces or in the flowing air, which has been well-documented (Filipić et al., 2020). The reduction of airborne PRRSv (in 50% tissue culture infective dose [$TCID_{50}$]) (Nayak et al., 2020), MS2 phage (Xia et al., 2019), and NDV (Schiappacasse et al., 2020) after plasma treatment reached 2.3, ~3.5, and ~3 logs, respectively. Meanwhile, the reduction of bacteria is usually 30–98%, lower than that of the virus. A possible reason is that bacteria have antioxidant systems such as superoxide dismutase and catalase enzymes to balance the exogenous ROS (Dharmaraja, 2017). Though less reported for air decontamination, the destruction of viral capsid protein and nucleic acid in the cases of surface and liquid disinfection by plasmas has been widely reported and mainly attributed to the oxidative stress caused by various RONS (Assadi et al., 2022). From this perspective, the plasma disinfector in this work is also promising for viral inactivation, which will be validated in our future work.

In terms of practical use, the DBD system used in this work can be improved in the following aspects. First, is the material of the holder. Organic materials are known to suffer from being etched by plasma species (Kuzminova et al., 2017), possibly releasing volatile harmful gases. Thus, inorganic or other safer materials could be used instead such as insulating glass, Al_2O_3, etc. Second, is the production of ozone, which is almost inevitable for all air-discharge-based plasma reactors. The feasible techniques for ozone removal may include catalysts, activated carbon filter (ACF), and photocatalysts (Batakliev et al., 2014; Namdari et al., 2021). Xia et al. reported a packed-bed plasma disinfector and they used a single layer of ACF to reduce the emitted ozone concentration from 2.25 to 0.09 ppm (Xia et al., 2019). In this work, we used the same method to reduce the emission of ozone. Under the applied voltage of 10 kVp and humidity of 40% at 1 m/s, the downstream ozone concentration is about 0.06 ppm (measured by an ozone analyzer), which is slightly lower than 160 μg/m^3 (~0.08 ppm), the 1-hour-average limit adopted by the Ambient Air Quality Standards of China (The Ministry of Environmental Protection of China, 2012). The filter has a pressure drop of 22 Pa at 1 m/s (12 Pa at 0.5 m/s). The combination of the plasma reactor and the filter yields a pressure drop of 40 Pa (16.5 Pa at 0.5 m/s), which is still lower than that of HEPA filters. Nevertheless, to achieve a lower pressure drop of ACF and also less ozone emission requires future efforts. Third, is long-term behavior of the system. The airborne particles are likely to accumulate on the dielectric surface through charging (Borra, 2008) or inertial impaction, which may lead to the disruption of discharge uniformity and thus the reduction of disinfection efficiency. In this regard, the parallel structure may be better because the discharge is confined in the region parallel to the major airflow. The vertical-2 reactor in this work has an accumulated usage time of ~60 h, during which we didn't observe any abnormalities. Thus, it requires a longer time to better evaluate the influence of particle accumulation.

5. Conclusions

In this work, the characteristics of grating-like DBD reactors were systemically evaluated. The tested reactor size and flow rates are suitable for practical use.

As indicated by the one-pass antibacterial performance tests, to enable direct contact of bacterial aerosol with discharge filaments, to increase injected discharge power by raising voltage (or frequency), and to increase the residence time of aerosol are fundamental keys to promoting bacterial inactivation efficiency. Experimental conditions, particularly humidity, can significantly influence the inactivation efficiency of DBD plasma. For the purpose of lower ozone concentration residues and higher inactivation efficiency, we suggest a RH range of 40%– 60%, which is also the typical indoor air-conditioned condition and can be easily achieved by a HAVC system. However, whether such a RH range is suitable for other forms of plasmas (e.g., packed-bed DBD) remains to be examined.

Species contributing most to airborne bacterial inactivation are gaseous short-lived ones, while the role of charged particles cannot be excluded. Long-lived species are dominated by O_3 and NO_2 and at most account for 30% of total inactivation. The chemical diagnosis of bacteria-containing droplets is of great significance to uncover the bactericidal mechanism. Also, the water contents in the bacteria-containing droplets may influence the performance of plasma treatment, which should be considered in the future research.

Environmental implication

DBD plasmas open a new door for fast and effective pathogen aerosol abatement in human-living environments, which is crucial in the context of spreading COVID-19.

CRediT authorship contribution statement

Liyang Zhang: Methodology, Investigation, Visualization, Writing – original draft. **Yuntao Guo:** Conceptualization, Investigation, Software, Writing – review & editing, Funding acquisition. **Xuanyu Chang:** Investigation, Resources. **Zenghui Yao:** Investigation, Formal analysis, Validation. **Xiaodong Wei:** Investigation, Resources. **Zihao Feng:** Investigation. **Dongheyu Zhang:** Investigation, Visualization. **Qun**

Zhou, Xinxin Wang, and **Haiyun Luo:** Funding acquisition, Conceptualization, Supervision.

Declaration of Competing Interest

The authors declare the following financial interests/personal relationships which may be considered as potential competing interests: Haiyun Luo reports financial support was provided by Tsinghua University Spring Breeze Fund. Yuntao Guo reports financial support was provided by China Postdoctoral Science Foundation. Haiyun Luo reports financial support was provided by Tsinghua University-Peking Union Medical College Hospital Initiative Scientific Research Program.

Acknowledgements

This work was funded by the Tsinghua University Spring Breeze Fund (2020Z99CFG007), China Postdoctoral Science Foundation (2021M701945), and Tsinghua University-Peking Union Medical College Hospital Initiative Scientific Research Program (20191080604).

Appendix A. Supporting information

Supplementary data associated with this article can be found in the online version at doi:10.1016/j.jhazmat.2022.129075.

References

Aboubakr, H., Gangal, U., Youssef, M., Goyal, S., Bruggeman, P., 2016. Inactivation of virus in solution by cold atmospheric pressure plasma: Identification of chemical inactivation pathways. J. Phys. D Appl. Phys. 49, 204001.
Assadi, I., Guesmi, A., Baaloudj, O., et al., 2022. Review on inactivation of airborne viruses using non-thermal plasma technologies: from MS2 to coronavirus. Environ. Sci. Pollut. Res. 29 (4), 4880–4892.
Azimi, P., Stephens, B., 2013. HVAC filtration for controlling infectious airborne disease transmission in indoor environments: Predicting risk reductions and operational costs. Build. Environ. 70, 150–160.
Batakliev, T., Georgiev, V., Anachkov, M., Rakovsky, S., Zaikov, G.E., 2014. Ozone decomposition. Inter. Toxicol. 7 (2), 47–59.
Bisag, A., Isabelli, P., Laurita, R., et al., 2020. Cold atmospheric plasma inactivation of aerosolized microdroplets containing bacteria and purified SARS-CoV-2 RNA to contrast airborne indoor transmission. Plasma Process. Polym. 17 (10), e2000154.
Blocken, B., van Druenen, T., Ricci, A., et al., 2021. Ventilation and air cleaning to limit aerosol particle concentrations in a gym during the COVID-19 pandemic. Build. Environ. 193, 107659.
Borra, J.P., 2008. Charging of aerosol and nucleation in atmospheric pressure electrical discharges. Plasma Phys. Control. Fusion 50 (12), 124036.
Chang, C.W., Li, S.Y., Huang, S.H., Huang, C.K., Chen, Y.Y., Chen, C.C., 2013. Effects of ultraviolet germicidal irradiation and swirling motion on airborne Staphylococcus aureus, Pseudomonas aeruginosa and Legionella pneumophila under various relative humidities. Indoor Air 23 (1), 74–84.
Chirokov, A., Gutsol, A., Fridman, A., Sieber, K.D., Grace, J.M., Robinson, K.S., 2004. Analysis of two-dimensional microdischarge distribution in dielectric-barrier discharges. Plasma Sources Sci. Technol. 13 (4), 623–635.
Deng, J., He, L., Zhao, B., Chen, Q., 2020. Effects of air relative humidity on spectral characteristics of dielectric barrier discharge plasma assisted combustion reactor. Vacuum 175, 109189.
Dharmaraja, A.T., 2017. Role of Reactive Oxygen Species (ROS) in Therapeutics and Drug Resistance in Cancer and Bacteria. J. Med Chem. 60 (8), 3221–3240.
Doležalová, E., Prukner, V., Lukeš, P., Šimek, M., 2016. Stress response of *Escherichia coli* induced by surface streamer discharge in humid air. J. Phys. D Appl. Phys. 49 (7), 075401.
Faulkner, C.A., Castellini, J.E., Zuo, W., Lorenzetti, D.M., Sohn, M.D., 2022. Investigation of HVAC operation strategies for office buildings during COVID-19 pandemic. Build. Environ. 207, 108519.
Feng, Z., Cao, S.-J., Wang, J., Kumar, P., Haghighat, F., 2021. Indoor airborne disinfection with electrostatic disinfector (ESD): Numerical simulations of ESD performance and reduction of computing time. Build. Environ. 200, 107956.
Filipić, A., Gutierrez-Aguirre, I., Primc, G., Mozetič, M., Dobnik, D., 2020. Cold plasma, a new hope in the field of virus inactivation. Trends Biotechnol. 38 (11), 1278–1291.
Fridman, A., Chirokov, A., Gutsol, A., 2005. Non-thermal atmospheric pressure discharges. J. Phys. D Appl. Phys. 38 (2), R1–R24.
Fujiyoshi, S., Tanaka, D., Maruyama, F., 2017. Transmission of airborne bacteria across built environments and its measurement standards: a review. Front. Microbiol. 8, 2336.
Gallagher Jr., M.J., Vaze, N., Gangoli, S., et al., 2007. Rapid inactivation of airborne bacteria using atmospheric pressure dielectric barrier grating discharge. IEEE Trans. Plasma Sci. 35 (5), 1501–1510.
Gao, H., Wang, G., Chen, B., et al., 2021. Atmospheric-pressure non-equilibrium plasmas for effective abatement of pathogenic biological aerosols. Plasma Sources Sci. Technol. 30 (5), 053001.
Ghimire, B., Lee, G.J., Mumtaz, S., Choi, E.H., 2018. Scavenging effects of ascorbic acid and mannitol on hydroxyl radicals generated inside water by an atmospheric pressure plasma jet. AIP Adv. 8 (7), 075021.
Guo, J., Huang, K., Wang, J., 2015. Bactericidal effect of various non-thermal plasma agents and the influence of experimental conditions in microbial inactivation: a review. Food Control 50, 482–490.
Guo, Y., Liu, P., Zhang, L., et al., 2021. Disinfection of Escherichia coli in ice by surface dielectric barrier discharge plasma. Appl. Phys. Lett. 119 (9), 090601.
Hähnel, M., von Woedtke, T., Weltmann, K.-D., 2010. Influence of the air humidity on the reduction of bacillus spores in a defined environment at atmospheric pressure using a dielectric barrier surface discharge. Plasma Process. Polym. 7 (3–4), 244–249.
Hwang, S.E., Chang, J.H., Oh, B., Heo, J., 2021. Possible aerosol transmission of COVID-19 associated with an outbreak in an apartment in Seoul, South Korea, 2020. Int. J. Infect. Dis. 104, 73–76.
Jiang, G., Wang, C., Song, L., et al., 2020. Aerosol transmission, an indispensable route of COVID-19 spread: case study of a department-store cluster. Front. Environ. Sci. Eng. 15 (3), 46.
Junhong, C., Pengxiang, W., 2005. Effect of relative humidity on electron distribution and ozone production by DC coronas in air. IEEE Trans. Plasma Sci. 33 (2), 808–812.
Ki, S.H., Masur, K., Baik, K.Y., Choi, E.H., 2019. Effects of humidity on room disinfection by dielectric barrier discharge plasma. J. Phys. D Appl. Phys. 52, 42.
Kim, D.-K., Kang, D.-H., Schottel Janet, L., 2018. UVC LED irradiation effectively inactivates aerosolized viruses, bacteria, and fungi in a chamber-type air disinfection system. Appl. Environ. Microbiol. 84 (17) e00944-18.
Kim, H.J., Han, B., Kim, Y.J., Oda, T., Won, H., 2013. Submicrometer particle removal indoors by a novel electrostatic precipitator with high clean air delivery rate, low ozone emissions, and carbon fiber ionizer. Indoor Air 23 (5), 369–378.
Kim, H.-J., Kim, M., Han, B., et al., 2019. Fine particle removal by a two-stage electrostatic precipitator with multiple ion-injection-type prechargers. J. Aerosol Sci. 130, 61–75.
Kogelheide, F., Voigt, F., Hillebrand, B., et al., 2020a. The role of humidity and UV-C emission in the inactivation of B. subtilis spores during atmospheric-pressure dielectric barrier discharge treatment. J. Phys. D Appl. Phys. 53 (29), 295201.
Komuro, A., Ono, R., Oda, T., 2013. Behaviour of OH radicals in an atmospheric-pressure streamer discharge studied by two-dimensional numerical simulation. J. Phys. D Appl. Phys. 46 (17), 175206.
Komuro, A., Ono, R., Oda, T., 2013b. Effects of pulse voltage rise rate on velocity, diameter and radical production of an atmospheric-pressure streamer discharge. Plasma Sources Sci. Technol. 22 (4), 045002.
Kuzminova, A., Kretkova, T., Kylian, O., et al., 2017. Etching of polymers, proteins and bacterial spores by atmospheric pressure DBD plasma in air. J. Phys. D Appl. Phys. 50 (13), 135201.
Lai, A.C.K., Cheung, A.C.T., Wong, M.M.L., Li, W.S., 2016. Evaluation of cold plasma inactivation efficacy against different airborne bacteria in ventilation duct flow. Build. Environ. 98, 39–46.
Lee, B., Bahnfleth, W.P., 2013. Effects of installation location on performance and economics of in-duct ultraviolet germicidal irradiation systems for air disinfection. Build. Environ. 67, 193–201.
Li, Y., Qian, H., Hang, J., 2021. Probable airborne transmission of SARS-CoV-2 in a poorly ventilated restaurant. Build. Environ. 196, 107788.
Liang, J.-l., Zheng, S.-h., Ye, S.-y., 2012. Inactivation of penicillium aerosols by atmospheric positive corona discharge processing. J. Aerosol Sci. 54, 103–112.
Liang, Y., Wu, Y., Sun, K., et al., 2012. Rapid inactivation of biological species in the air using atmospheric pressure nonthermal plasma. Environ. Sci. Technol. 46 (6), 3360–3368.
Liu, Z.C., Liu, D.X., Chen, C., et al., 2015. Physicochemical processes in the indirect interaction between surface air plasma and deionized water. J. Phys. D Appl. Phys. 48 (49), 495201.
Lukes, P., Dolezalova, E., Sisrova, I., Clupek, M., 2014. Aqueous-phase chemistry and bactericidal effects from an air discharge plasma in contact with water: evidence for the formation of peroxynitrite through a pseudo-second-order post-discharge reaction of H2O2and HNO2. Plasma Sources Sci. Technol. 23 (1), 015019.
Luo, H., Zhong, L., 2021. Ultraviolet germicidal irradiation (UVGI) for in-duct airborne bioaerosol disinfection: review and analysis of design factors. Build. Environ. 197, 107852.
Mihai, V., Rusu, L., 2021. An overview of the ship ventilation systems and measures to avoid the spread of diseases. Inventions 6 (3).
Miller, S.L., Nazaroff, W.W., Jimenez, J.L., et al., 2021. Transmission of SARS-CoV-2 by inhalation of respiratory aerosol in the Skagit Valley Chorale superspreading event. Indoor Air 31 (2), 314–323.
Mo, J., Tian, E., Pan, J., 2020. New electrostatic precipitator with dielectric coatings to efficiently and safely remove sub-micro particles in the building environment. Sustain. Cities Soc. 55, 102063.
Moldgy, A., Nayak, G., Aboubakr, H.A., Goyal, S.M., Bruggeman, P.J., 2020. Inactivation of virus and bacteria using cold atmospheric pressure air plasmas and the role of reactive nitrogen species. J. Phys. D Appl. Phys. 53 (43), 434004.
Möritz, M., Peters, H., Nipko, B., Rüden, H., 2001. Capability of air filters to retain airborne bacteria and molds in heating, ventilating and air-conditioning (HVAC) systems. Int. J. Hyg. Environ. Health 203 (5), 401–409.
Nakagawa, Y., Ono, R., Oda, T., 2011. Density and temperature measurement of OH radicals in atmospheric-pressure pulsed corona discharge in humid air. J. Appl. Phys. 110 (7), 073304.

Namdari, M., Lee, C.-S., Haghighat, F., 2021. Active ozone removal technologies for a safe indoor environment: A comprehensive review. Build. Environ. 187, 107370.
Nayak, G., Andrews, A.J., Marabella, I., et al., 2020. Rapid inactivation of airborne porcine reproductive and respiratory syndrome virus using an atmospheric pressure air plasma. Plasma Process. Polym. 17 (10), e1900269.
Nelson, D., Benhenni, M., Eichwald, O., Yousfi, M., 2003. Ion swarm data for electrical discharge modeling in air and flue gas mixtures. J. Appl. Phys. 94 (1), 96–103.
Nguyen, D.B., Shirjana, S., Hossain, M.M., Heo, I., Mok, Y.S., 2020. Effective generation of atmospheric pressure plasma in a sandwich-type honeycomb monolith reactor by humidity control. Chem. Eng. J. 401, 125970.
Park, C.W., Hwang, J., 2013. Susceptibility constants of airborne bacteria to dielectric barrier discharge for antibacterial performance evaluation. J. Hazard. Mater. 244, 421–428.
Patil, S., Moiseev, T., Misra, N.N., et al., 2014. Influence of high voltage atmospheric cold plasma process parameters and role of relative humidity on inactivation of Bacillus atrophaeus spores inside a sealed package. J. Hosp. Infect. 88 (3), 162–169.
Pavlovich, M.J., Clark, D.S., Graves, D.B., 2014. Quantification of air plasma chemistry for surface disinfection. Plasma Sources Sci. Technol. 23 (6), 065036.
Pease, L.F., Wang, N., Salsbury, T.I., et al., 2021. Investigation of potential aerosol transmission and infectivity of SARS-CoV-2 through central ventilation systems. Build. Environ. 197, 107633.
Prehn, F., Timmermann, E., Kettlitz, M., Schaufler, K., Guenther, S., Hahn, V., 2020. Inactivation of airborne bacteria by plasma treatment and ionic wind for indoor air cleaning. Plasma Process. Polym. 17 (9), e2000027.
Qiao, Y., Yang, M., Marabella, I.A., et al., 2021. Greater than 3-Log Reduction in Viable Coronavirus Aerosol Concentration in Ducted Ultraviolet-C (UV–C) Systems. Environ. Sci. Technol. 55 (7), 4174–4182.
Ran, J., Li, C., Ma, D., Luo, H., Li, X., 2018. Homogeneous dielectric barrier discharges in atmospheric air and its influencing factor. Phys. Plasmas 25 (3), 033511.
Ren, Y.-F., Huang, Q., Marzouk, T., et al., 2021. Effects of mechanical ventilation and portable air cleaner on aerosol removal from dental treatment rooms. J. Dent. 105, 103576.
World Health Organization, 2020. Transmission of SARS-CoV-2: Implications for Infection Prevention Precautions: Scientific Brief. ⟨https://apps.who.int/iris/handle/10665/333114⟩; ⟨WHO/2019-nCoV/Sci_Brief/Transmission_modes/2020.3⟩. (Accessed 9 July 2020).
The Standardization Administration of the People's Republic of China, 2017. Air cleaner for ventilation system (in Chinese). ⟨http://www.gb688.cn/bzgk/gb/newGbInfo?hcno=6E47BDF2B375D33869EA7265F4818D64⟩. (Accessed 1 September 2021).
World Health Organization, 2021. Roadmap to improve and ensure good indoor ventilation in the context of COVID-19. ⟨https://www.who.int/publications/i/item/9789240021280⟩. (Accessed 25 February 2022).
Romero-Mangado, J., Dey, A., Diaz-Cartagena, D.C., et al., 2017. Efficacy of atmospheric pressure dielectric barrier discharge for inactivating airborne pathogens. J. Vac. Sci. Technol. A 35 (4), 041101.
Romero-Mangado, J., Nordlund, D., Soberon, F., et al., 2016. Morphological and chemical changes of aerosolized E. coli treated with a dielectric barrier discharge. Biointerphases 11 (1), 011009.
Sakiyama, Y., Graves, D.B., Chang, H.-W., Shimizu, T., Morfill, G.E., 2012. Plasma chemistry model of surface microdischarge in humid air and dynamics of reactive neutral species. J. Phys. D Appl. Phys. 45 (42), 425201.
Schiappacasse, C., Peng, P., Zhou, N., et al., 2020. Inactivation of aerosolized newcastle disease virus with non-thermal plasma. Appl. Eng. Agric. 36 (1), 55–60.
Staack, D., Farouk, B., Gutsol, A., Fridman, A., 2005. Characterization of a dc atmospheric pressure normal glow discharge. Plasma Sources Sci. Technol. 14 (4), 700–711.
Staack, D., Farouk, B., Gutsol, A., Fridman, A., 2005. Characterization of a dc atmospheric pressure normal glow discharge. Plasma Sources Sci. Technol. 14, 700–711.
Takaki, K., Miura, T., Oka, A., Takahashi, K., 2021. Influence of relative humidity on ethylene removal using dielectric barrier discharge. IEEE Trans. Plasma Sci. 49 (1), 61–68.
Tang, S., Mao, Y., Jones, R.M., et al., 2020. Aerosol transmission of SARS-CoV-2? Evidence, prevention and control. Environ. Int. 144, 106039.
Tian, W., Kushner, M.J., 2014. Atmospheric pressure dielectric barrier discharges interacting with liquid covered tissue. J. Phys. D Appl. Phys. 47 (16), 165201.
van Doremalen, N., Bushmaker, T., Morris, D.H., 2020. Aerosol and surface stability of SARS-CoV-2 as compared with SARS-CoV-1. N. Engl. J. Med. 382 (16), 1564–1567.
Vaze, N.D., Gallagher, M.J., Park, S., et al., 2010. Inactivation of bacteria in flight by direct exposure to nonthermal plasma. IEEE Trans. Plasma Sci. 38 (11), 3234–3240.
Vernez, D., Schwarz, S., Sauvain, J.-J., Petignat, C., Suarez, G., 2021. Probable aerosol transmission of SARS-CoV-2 in a poorly ventilated courtroom. Indoor Air 31 (6), 1776–1785.
Walker, C.M., Ko, G., 2007. Effect of ultraviolet germicidal irradiation on viral aerosols. Environ. Sci. Technol. 41 (15), 5460–5465.
Wang, C.C., Prather, K.A., Sznitman, J., et al., 2021. Airborne transmission of respiratory viruses. Science 373 (6558), 958–961.
Winter, J., Tresp, H., Hammer, M.U., et al., 2014. Tracking plasma generated H_2O_2 from gas into liquid phase and revealing its dominant impact on human skin cells. J. Phys. D Appl. Phys. 47 (28), 285401.
Wu, H., Sun, P., Feng, H., et al., 2012. Reactive oxygen species in a non-thermal plasma microjet and water system: generation, conversion, and contributions to bacteria inactivation-an analysis by electron spin resonance spectroscopy. Plasma Process. Polym. 9 (4), 417–424.
Wu, Y., Liang, Y., Wei, K., 2015. MS2 virus inactivation by atmospheric-pressure cold plasma using different gas carriers and power levels. Appl. Environ. Microbiol. 81 (3), 996.
Xi, W., Wang, W., Liu, Z., et al., 2020. Mode transition of air surface micro-discharge and its effect on the water activation and antibacterial activity. Plasma Sources Sci. Technol. 29 (9), 095013.
Xia, T., Kleinheksel, A., Lee, E.M., Qiao, Z., Wigginton, K.R., Clack, H.L., 2019. Inactivation of airborne viruses using a packed bed non-thermal plasma reactor. J. Phys. D Appl. Phys. 52 (25), 255201.
Xia, T., Yang, M., Marabella, I., et al., 2020. Inactivation of airborne porcine reproductive and respiratory syndrome virus (PRRSv) by a packed bed dielectric barrier discharge non-thermal plasma. J. Hazard Mater. 393, 122266.
Xiang, J., Huang, C.-H., Austin, E., Shirai, J., Liu, Y., Seto, E., 2021. Energy consumption of using HEPA-based portable air cleaner in residences: a monitoring study in Seattle, US. Energy Build. 236, 110773.
Zaatari, M., Novoselac, A., Siegel, J., 2014. The relationship between filter pressure drop, indoor air quality, and energy consumption in rooftop HVAC units. Build. Environ. 73, 151–161.
Zhang, H., Jin, X., Nunayon, S.S., Lai, A.C.K., 2020. Disinfection by in-duct ultraviolet lamps under different environmental conditions in turbulent airflows. Indoor Air 30 (3), 500–511.
Zhang, L., Wang, H., Luo, H., 2020. Uncovering the inactivation kinetics of Escherichia coli in saline by atmospheric DBD plasma using ATR FT-IR. Plasma Process. Polym. 17 (9), 1900197.
Zhang, L., Zhang, D., Guo, Y., Peng, S., Zhou, Q., Luo, H., 2021. In situ FTIR spectroscopy study on biomolecular etching by atmospheric pressure plasma jets. J. Phys. D Appl. Phys. 54 (46), 465204.
Zhang, S., Wang, W.-C., Jiang, P.-C., Yang, D.-z, Jia, L., Wang, S., 2013. Comparison of atmospheric air plasmas excited by high-voltage nanosecond pulsed discharge and sinusoidal alternating current discharge. J. Appl. Phys. 114 (16), 163301.
Zhang, X., Lee, B.J., Im, H.G., Cha, M.S., 2016. Ozone production with dielectric barrier discharge: effects of power source and humidity. IEEE Trans. Plasma Sci. 44 (10), 2288–2296.
Ambient air quality standards, 2012. The Ministry of Environmental Protection of China. https://www.transportpolicy.net/standard/china-air-quality-standards/?title=china:_air_quality_standards#GB_3095-2012. (Accessed 10 April 2022).